Original Article

Journal of
LOW FREQUENCY
NOISE, VIBRATION
AND ACTIVE CONTROL

Journal of Low Frequency Noise,
Vibration and Active Control
2023, Vol. 42(4) 1821–1836

DOI: 10.1177/14613484231186695
journals.sagepub.com/home/lfn
Sage

Research on control strategy of an active magnetorheological fluid bearing based on improved gray wolf optimization approach

Lai Peng[1], Dezheng Hua[1], Xinhua Liu[1], Darius Andriukaitis[2], Grzegorz Królczyk[3] and Zhixiong Li[3]

Abstract

In order to address the problems of insufficient load capacity and rotor vibration, an active fluid-film bearing lubricated with magnetorheological fluid (MRF) is proposed. First, the geometry of the MRF fluid-film bearing is designed and its intelligent lubrication mechanism is analyzed to clarify its advantages. In addition, mathematical model of MRF fluid-film bearing-rotor system is derived, and FEM model is utilized to obtain stiffness and damping coefficients to supplement mathematical model. Moreover, an improved gray wolf optimization (IGWO) algorithm is developed to tune the PID controller parameters. The validity of the proposed method is verified by numerical simulation. Furthermore, the simulation results show that with the increasing of current magnitude, the orbits of shaft center decrease. Under the presence of magnetic fields, the shaft center orbits of the MRF bearing can converge to a point, and therefore this bearing has ability to suppress rotor vibration. Finally, IGWO-PID controller has better response characteristics than GWO, PSO, and GA algorithms, and hence the IGWO algorithm can find the more appropriate PID controller parameters, that the validity of the improved algorithm is further proved. Therefore, the active bearing and its research findings provide new reference for MRF vibration control in the field of journal bearing lubrication.

Keywords

Magnetorheological fluid, fluid-film bearing, intelligent lubrication, improved gray wolf optimizer, multi-physics field simulation, Proportional-Integral-Derivative controller

Introduction

Fluid-film bearings are widely used in industry for applications of rotating machines.[1,2] Apart from having a long service life, their capability to cause low shear levels and to support high payload show the advantages of using them. Although these advantages, the researchers are striving to improve their performance to meet new requirements under different operating conditions.[3,4] Through reading literature and actual investigations, the design of new bearing concepts,[5,6] bearing geometries,[7,8] and new lubricants[9,10,11,12] are some approaches to increase performance of fluid-film bearing. Magnetorheological fluids (MRF) capable of controllable and reversible rheological properties are widely used in brakes,[13,14] medical instruments,[15,16] dampers,[17,18] sealings,[19,20] and other engineering fields.[21,22] As a result, MRF as intelligent lubrication medium is applied to bearing to obtain the superior controllable performance under different operating situations.

[1]School of Mechatronic Engineering, China University of Mining and Technology, Xuzhou, China
[2]Department of Electronics Engineering, Kaunas University of Technology, Kaunas, Lithuania
[3]Faculty of Mechanical Engineering, Opole University of Technology, Opole, Poland

Corresponding authors:
Xinhua Liu, China University of Mining and Technology,Xuzhou, China; Zhixiong Li, Opole University of Technology, 45-758 Opole, Poland.
Emails: liuxinhua@cumt.edu.cn; z.li@po.edu.pl

Data Availability Statement included at the end of the article

The work of Hesselbach and Guldbakke[23,24] was the first to apply MRF into hydrostatic bearing lubrication. Under different payloads, their hydrostatic thrust bearing was able to maintain a constant gap with the help of MRF behavior. In addition, by experimental validation, it is concluded that it would achieve quasi-infinite stiffness in the closed loop control, and quicker response than conventional valve control system. In the study of hydrodynamic bearing lubricated with MRF, Furthermore, Gertzos et al.,[25] Bompos et al.,[26] and Sahu et al.[27] studied the operating parameters and pressure distribution of MRF fluid-film through numerical codes and hydrodynamic lubrication model. Researchers studied the difference between MRF and ferrofluid lubrication performance in fluid-film bearing.[28,29] Compared with MRF, ferrofluid needs stronger current to achieve the same viscosity. Therefore, the energy consumption of MRF is lower than ferrofluid. As a result, the MRF in bearing application can have more advantages and better performances. Moreover, Bompos et al.[30,31] and Wang et al.[32,33] studied dynamic coefficients of the hydrodynamic bearing lubricated with MRF, whose tunable characteristics are responsible for the enhanced carrying capacity. Although higher friction losses are observed in the hydrodynamic bearing lubricated with MRF compared to the traditional lubricant oil, this work has verified that the fluid-film is thicker at low speed and pressure distribution is beneficial to supporting the heavier payloads.[34] Finally, Urreta and his research team[35] showed that 50 % higher load capacities and bigger stiffnesses were experimental demonstrated in the hybrid journal bearing, and good hydrodynamic responses had not been showed in the active lubrication based on magnetorheological valves, which were used to control the flow rate of MRF with PID controller according to the rotor track. Despite it was demonstrated that MRF hydrodynamic bearing has better hydrodynamic performance and load capacity than traditional fluid-film bearing, little attention has been paid to active fluid-film bearing to further improve the hydrodynamic bearing performance.

Control algorithms are widely used in the field of automatic control field,[36,37] PID algorithm is one of useful control algorithms.[38,39] It has been widely used in the active magnetic bearing control system and is usually used as the main controller of the system.[40,41] Jonathan et al.[42] used particle swarm optimization (PSO) algorithm to optimize PID parameters and the performance of active magnetic bearing is evaluated. In addition, Bordoloi et al.[43] adopted genetic algorithm (GA) for the optimization of PID controller parameters in active magnetic bearing. Finally, Gupta et al.[44] utilized individually ant lion optimization (ALO), gray wolf optimization (GWO), and whale optimization algorithm (WOA) to calculate the gain parameters of the PID controller in magnetic bearing. It is reasonable to apply the GWO method to bearing radius clearance control; however, GWO has not been reported for vibration suppression in existing MRF bearing system yet. The reason is that GWO algorithm cannot be directly applied to a specific MRF bearing, and hence it is necessary to improve GWO algorithm to make it suitable for controller parameters optimization of the active MRF bearing. Because most of existing MRF bearing research focuses on the structure, functional design and identification of stiffness and damping coefficients, very limited work has considered precise orbit control in the MRF bearing design process. As a result, it is worth integrating a GWO-based controller into an active MRF bearing to make it ready for practical usage; especially in the high-precision machine tool application where MRF bearing is required to intelligently adapt to more critical operating conditions to enhance machining accuracy of workpiece.

A novel MRF fluid-film bearing based on an IGWO-PID controller is proposed in this work. First, the MRF fluid-film bearing is designed, and its intelligent lubrication mechanism is analyzed clarify its advantages. In addition, mathematical model of MRF fluid-film bearing-rotor system is derived, and FEM model is utilized to obtain stiffness and damping coefficients to supplement mathematical model. Moreover, an improved grey wolf optimization (IGWO) algorithm is developed to tune the PID parameters. The validity of the proposed method is verified by numerical simulation. Lastly, the simulation results show that with the increasing of current magnitude, the orbits of shaft center decrease. The shaft center orbits of the active MRF bearing can converge to a point in the action of external magnetic field. Finally, IGWO-PID controller has better response characteristics than GWO, PSO, and GA algorithms, and hence the IGWO algorithm can find the more appropriate PID controller parameters, that the validity of this algorithm is further proved.

The remainder of this paper is organized as follows. The structural design and mechanism of the MRF lubrication bearing are described and mathematical model of bearing-rotor system is derived in Section 2. In Section 3, the improved GWO algorithm is proposed, and its feasibility is verified. The simulations are carried out to verify that proposed bearing has better load capacity and smaller orbits of shaft center than traditional fluid-film bearing, and the proposed IGWO-PID controller parameters have better response characteristics in section 4. Conclusions and future works are summarized in section 5.

Theoretical model and methods

Geometric model of bearing lubricated with m

In this work, the characteristics of magnetorheological fluid are analyzed and utilized as lubricant in the bearing. The particles of MR fluid are in a disordered state in the absence of external magnetic field. While under the action of the

magnetic field, the particles have an obvious orientation trend along the direction of the magnetic field.[45,46] By changing the external magnetic field, the viscosity of the MR fluid can be adjusted freely.

Figure 1 shows the distribution of the magnetic particles in the radius gap. From Figure 1(a), while rotor is rotating at speed ω, magnetic particles show a normal distribution in the carrier fluid. However, due to the presence of a magnetic field, magnetic particles align along the direction of the magnetic field to form a chain-like structure in the Figure 1(b). In addition, particle chains are inclined because of the shear motion of rotor. As a result, the viscosity of MRF is dramatically increased, which offers enormous damping and stiffness, and therefore the MRF bearing can provide greater hydrodynamic pressure and hold up shaft more easily than traditional fluid-film bearing.

Applied cooperation between magnetorheological fluid and fluid-film bearing, a novel active fluid-film bearing lubricated with magnetorheological fluid is proposed in this research. As shown in Figure 2(a), it consists of bearing, shaft, silicon steel sheets, and coil, which is wound around a silicon steel sheets and excited by DC power to produce magnetic field. The narrow radius clearance between bearing and shaft fills up with magnetorheological fluid, which can avoid friction between them. The main structural parameters of bearing and magnetorheological fluid are shown in Table 1. This work using magnetorheological fluid is MRF-132DG produced by Lord corporation,[47] which is formulated for general use in controllable, energy-dissipating application such as shocks, dampers, and brakes.

Figure 2(b) presents an overview of the bearing control system. When shaft is driven by motor at ω speed, the lubricant is dragged into the narrow gap between shaft and bearing, and hence hydrodynamic pressure in the fluid film is generated. If the hydrodynamic pressure of the lubricant is high enough to support the shaft, it can avoid the direct contact between shaft and bearing and reduce friction. Due to the increased viscosity of MRF under the presence of magnetic field, it is extremely easy to increase the pressure and avoid the direct contact between shaft and bearing. Thus, contact and friction between them can be reduced, and their service time could be prolonged. Specifically, the displacement signal of the shaft is measured by the two eddy current sensors, and then is delivered to the signal processing. After filtering and compensation, we can clearly observe the movement locus of the shaft on the screen. The method of synthetic track can be expressed as

$$\begin{cases} x = Ae^{j(\omega t+\alpha)} \\ y = Be^{j(\omega t+\beta)} \end{cases} \tag{1}$$

where x and y are vectors measured by displacement sensors, A and B represent amplitude of the vectors, and α and β are the phases of vectors.

Hydrodynamic force of bearing lubricated with MRF

Hydrodynamic force equation. The differential equation for governing the flow of fluid in the hydrodynamic bearing is expressed as

$$\frac{\partial}{\partial x}\left[\frac{h^3\partial p}{\mu\,\partial x}\right]+\frac{\partial}{\partial z}\left[\frac{h^3\partial p}{\mu\,\partial z}\right]=6U\frac{\partial h}{\partial x} \tag{2}$$

where x and z are circumferential and axial coordinates, respectively, μ represents dynamic viscosity of the fluid, h denotes fluid-film thickness at any point, p is the pressure distribution of fluid, and U represents linear velocity of the rotor.

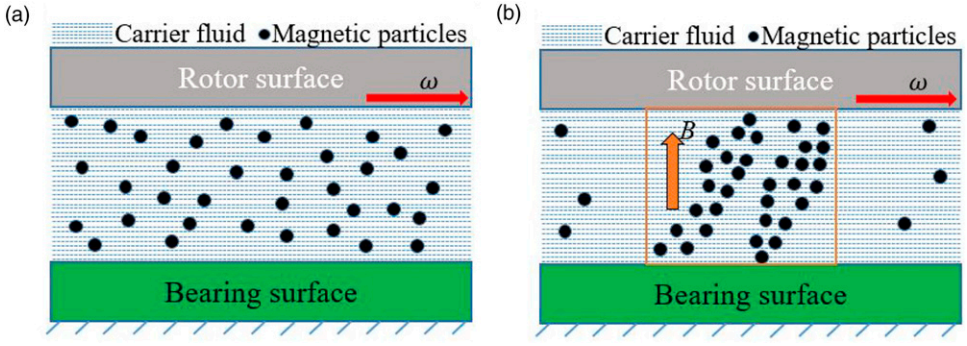

Figure 1. Magnetic particles motion in the radius gap. (a) No magnetic field is applied. (b) Magnetic field is applied.

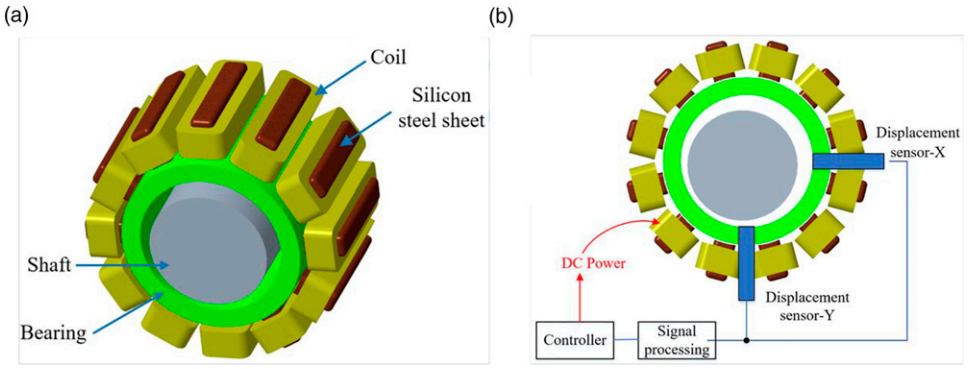

Figure 2. Model of the active bearing lubricated with magnetorheological fluid. (a) 3-D structural model of the bearing. (b) Overview of the bearing control system.

Table 1. Main parameters of bearing and MRF.

Structural parameters	Value	MRF parameters	Value
Diameter of the shaft (D)	60 mm	Viscosity	0.11 Pa • s
Length of bearing (L)	60 mm	Density	2.95 g/cm^3
Radius clearance (C)	0.1 mm	Solids content by weight	80.95%
Number of turns of coil	400	Operating temperature	−40 ~ +130 °C

By solving the above formula, we can obtain the pressure distribution p. Loading capacity that is exceedingly important parameter of oil film bearing is obtained. The hydrodynamic forces are as follows

$$F_x = -\int_0^L \int_0^{\pi D} psin\,\varphi dxdz \tag{3}$$

$$F_y = -\int_0^L \int_0^{\pi D} pcos\,\varphi dxdz \tag{4}$$

$$F = \sqrt{F_x^2 + F_y^2} \tag{5}$$

where F is loading capacity, F_x and F_y are components of loading capacity in the x and y axis accordingly.

Similarly, for the dynamic performance of the bearing, Figure 3 is two direct and two cross-coupled, that is, 2 × 2 the stiffness and damping coefficients, and the specific matrices can be calculated

$$\begin{bmatrix} K_{xx} & K_{xy} \\ K_{yx} & K_{yy} \end{bmatrix} = \begin{bmatrix} \frac{\partial F_x}{\partial x} & \frac{\partial F_x}{\partial y} \\ \frac{\partial F_y}{\partial x} & \frac{\partial F_y}{\partial y} \end{bmatrix} = -\begin{bmatrix} \frac{\partial}{\partial x}\int_0^L \int_0^{\pi D} psin\,\varphi dxdz & \frac{\partial}{\partial y}\int_0^L \int_0^{\pi D} psin\,\varphi dxdz \\ \frac{\partial}{\partial x}\int_0^L \int_0^{\pi D} pcos\,\varphi dxdz & \frac{\partial}{\partial y}\int_0^L \int_0^{\pi D} pcos\,\varphi dxdz \end{bmatrix}, \tag{6}$$

$$\begin{bmatrix} C_{xx} & C_{xy} \\ C_{yx} & C_{yy} \end{bmatrix} = \begin{bmatrix} \frac{\partial F_x}{\partial \dot{x}} & \frac{\partial F_x}{\partial \dot{y}} \\ \frac{\partial F_y}{\partial \dot{x}} & \frac{\partial F_y}{\partial \dot{y}} \end{bmatrix} = -\begin{bmatrix} \frac{\partial}{\partial \dot{x}}\int_0^L \int_0^{\pi D} psin\,\varphi dxdz & \frac{\partial}{\partial \dot{y}}\int_0^L \int_0^{\pi D} psin\,\varphi dxdz \\ \frac{\partial}{\partial \dot{x}}\int_0^L \int_0^{\pi D} pcos\,\varphi dxdz & \frac{\partial}{\partial \dot{y}}\int_0^L \int_0^{\pi D} pcos\,\varphi dxdz \end{bmatrix}, \tag{7}$$

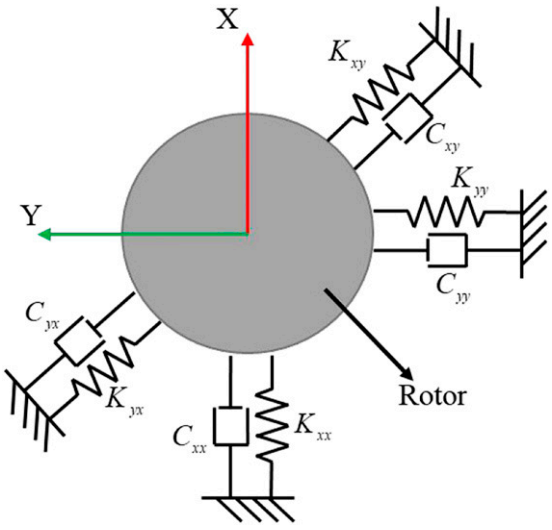

Figure 3. The bearing stiffness and damping coefficients.

where K_{ii} is the stiffness coefficient and C_{jj} is the damping coefficient, and they can be obtained from FEM simulation in this work, φ is pressure angle.

Constitute equation for MRF. In this work, the viscosity of MRF can be approximated with the Bingham law for yield stress

$$\tau = \tau_0(H) + \eta_0\dot{\gamma} \tag{8}$$

where τ is the shear stress of the material, τ_0 is the critical shear stress or yield stress, η_0 is viscosity of MRF without magnetic field, and $\dot{\gamma}$ is the shear rate.

As provided by Lord Corp., the *B-H* and shear yield stress relationships for the MRF used (MRF-132DG) can be found in.Ref [44] Through curve fitting, the magnetic field strength H can be described accurately in terms of the magnetic induction intensity B (T) of this material by the following cubic

$$H(B) = 0.6168B^3 + 278.718B^2 + 14.29B + 6.98\,[\mathrm{kA/m}] \tag{9}$$

To relate the magnetic field strength to the yield behavior of the material, the shear yield stress τ_0 can be expressed in terms of H with a quadratic fit

$$\tau_0(H) = -0.745H^2 + 382.868H - 1623.59\,[\mathrm{pa}] \tag{10}$$

Both sides of equation (8) are divided by the shear rate $\dot{\gamma}$, and this equation can also be converted into

$$\eta = \eta_0 + \tau_0(H)/\dot{\gamma}\ [\mathrm{pa}.s] \tag{11}$$

As a result, the different viscosity under various magnetic fields can be obtained easily to simulate the MRF effect in bearing lubrication.

Mathematical model of MRF bearing-rotor system

In this work, since the rotor speed is far lower than the bending critical speed, it can be modeled as a rigid body. As shown in Figure 4, this system consists of a shaft, two bearings and a disk, which is in the middle of two bearings. The gap between rotor and bearing is filled with MR fluid. Since hydrodynamic bearing is modeled as stiffness and damping coefficients matrices, the equations are as follows

$$\begin{cases} \frac{1}{2}m_r\ddot{x}_c + c_{xx}\dot{x}_c + c_{xy}\dot{y}_c + k_{xx}x_c + k_{xy}y_c = 0 \\ \frac{1}{2}m_r\ddot{y}_c + c_{yx}\dot{x}_c + c_{yy}\dot{y}_c + k_{yx}x_c + k_{yy}y_c = \frac{1}{2}mg + \frac{1}{2}W \\ J_x\ddot{\theta}_x + J_z\omega\dot{\theta}_y = 0 \\ J_y\ddot{\theta}_y - J_z\omega\dot{\theta}_x = 0 \end{cases} \tag{12}$$

where m_r is mass of rotor, m is expressed as $m = m_d + m_r$, m_d represents the mass of the disk, W denotes the external load, J_x, J_y, and J_z are the moment of inertia of the rotor about the X axis, Y axis, and Z axis at the center of mass, respectively, and ω is the angular speed of rotor rotation.

Furthermore, since the two bearings are symmetrical about the center of mass, two equations can be obtained: $F_{x1} = F_{x2}$, $F_{y1} = F_{y2}$. Equation (11) is also written as

$$M\ddot{q}_c + (C + \omega G)\dot{q}_c + Kq_c = u \tag{13}$$

where $q_c = [x_c \quad y_c \quad \theta_x \quad \theta_y]^T$, $u = \left[0 \quad \frac{1}{2}mg + \frac{1}{2}W \quad 0 \quad 0\right]^T$, M is mass matrix, C represents damping matrix, G denotes gyroscopic matrix, and the above three matrices are given as

$$M = \begin{bmatrix} \frac{1}{2}m_r & 0 & 0 & 0 \\ 0 & \frac{1}{2}m_r & 0 & 0 \\ 0 & 0 & J_x & 0 \\ 0 & 0 & 0 & J_y \end{bmatrix}, G = \begin{bmatrix} 0 & 0 & 0 & 0 \\ 0 & 0 & 0 & 0 \\ 0 & 0 & 0 & J_z \\ 0 & 0 & -J_z & 0 \end{bmatrix} \tag{14}$$

$$C = \begin{bmatrix} C_1 & O_{2\times2} \\ O_{2\times2} & O_{2\times2} \end{bmatrix}, K = \begin{bmatrix} K_1 & O_{2\times2} \\ O_{2\times2} & O_{2\times2} \end{bmatrix} \tag{15}$$

where $C_1 = \begin{bmatrix} c_{xx} & c_{xy} \\ c_{yx} & c_{yy} \end{bmatrix}$ and $K_1 = \begin{bmatrix} k_{xx} & k_{xy} \\ k_{yx} & k_{yy} \end{bmatrix}$, which can be obtained by equations (6) and (7).

Moreover, x_1, x_2, y_1, and y_2 are defined as the displacement of the rotor at the left and right bearing lubricated with MRF. Currently, q_c and displacement of rotor have the following transformation relationship

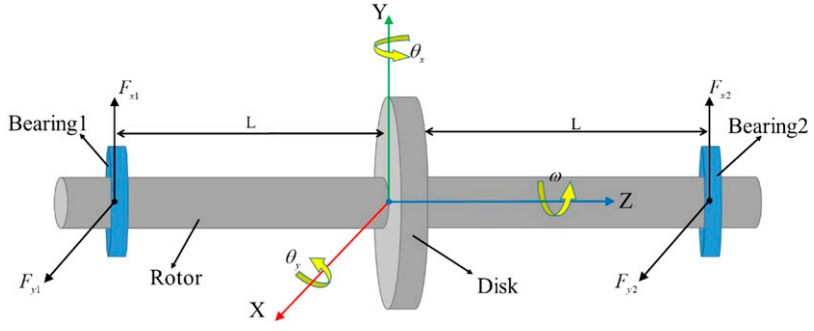

Figure 4. Schematic view of rotor-bearing system.

$$\begin{cases} x_c = \frac{1}{2}x_1 + \frac{1}{2}x_2 \\ y_c = \frac{1}{2}y_1 + \frac{1}{2}y_2 \\ \theta_x = \frac{1}{2L}y_1 - \frac{1}{2L}y_2 \\ \theta_y = \frac{-1}{2L}x_1 + \frac{1}{2L}x_2 \end{cases}, q_c = \frac{1}{2}\begin{bmatrix} 1 & 0 & 1 & 0 \\ 0 & 1 & 0 & 1 \\ 0 & \frac{1}{L} & 0 & -\frac{1}{L} \\ \frac{-1}{L} & 0 & \frac{1}{L} & 0 \end{bmatrix} Y \tag{16}$$

where $Y = [x_1 \quad y_1 \quad x_2 \quad y_2]^T$, and equation (15) is also expressed as: $q_c = T_r Y$, and hence equation (12) can be transformed as

$$MT_r\ddot{Y} + (C + \omega G)T_r\dot{Y} + KT_rY = u \tag{17}$$

The bearing-rotor system state space equation can be written as

$$\begin{cases} \dot{Z} = A_sZ + B_su \\ Y = C_sZ + D_su \end{cases} \tag{18}$$

where $A_s = \begin{bmatrix} O_{4\times4} & I_{4\times4} \\ -(MT_r)^{-1}KT_r & -(MT_r)^{-1}(C + \omega G)T_r \end{bmatrix}$, $B_s = \begin{bmatrix} O_{4\times4} \\ (MT_r)^{-1} \end{bmatrix}$, $C_s = [I_{4\times4} \quad O_{4\times4}]$, $D_s = O_{4\times4}$, u is input vector, $Z = [x_1 \quad y_1 \quad x_2 \quad y_2 \quad \dot{x}_1 \quad \dot{y}_1 \quad \dot{x}_2 \quad \dot{y}_2]^T$ is state vector, $Y = [x_1 \quad y_1 \quad x_2 \quad y_2]^T$ is output vector.

Finite element model simulation

As for the considerations that it went into the design and analysis of the active MRF bearing-rotor system, a 3D model was developed in the FEM software COMSOL Multiphysics version 6.0. In this simulation, four physical field modules were used, which are magnetic field, hydrodynamic bearing, beam rotor and multi-physics, respectively. Figure 5 is 3D model of bearing-rotor system in this FEM software. Induced magnetic field is generated by coil, which has influence on MRF in the hydrodynamic bearing. Moreover, the coupling of hydrodynamic bearing and magnetic field was solved through stationary study, where coil geometry analysis was indispensable. The Multiphysics included hydrodynamic bearing and beam rotor, which was solved through time dependent. Besides, beam rotor module simplified the rotor and disk model by the data setting. The numerical parameters, needed to model the bearing-rotor system, are detailed in Table 2.

Transfer functions of bearing-rotor system

In this work, we utilized Y-axis displacement of rotor as output. The transfer functions of this complex system integrated machinery, electric, fluid drive and control engineering are composed of two parts: one is current transformed into hydrodynamic force, and the other is the influence of hydrodynamic force on mechanical system. The complete control system is shown in Figure 11.

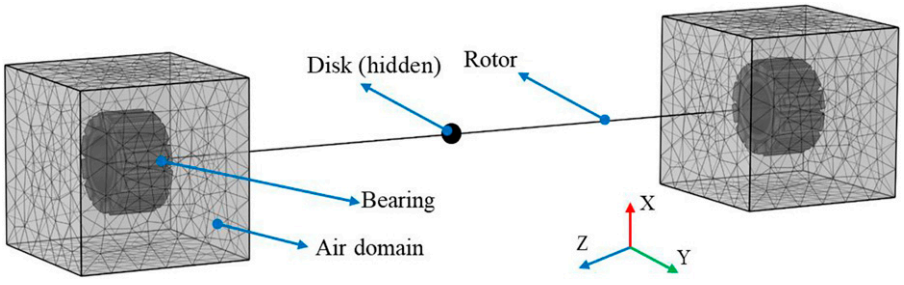

Figure 5. 3D FEM model of rotor-bearing system.

Table 2. The numerical parameters in FEM model.

Parameter	Materials	Parameter	Value
Bearing	Bronze	Rotor length (L_r)	0.9 m
Coil	Copper	Density of rotor and disk (ρ)	7800 kg/m^3
Silicone steel sheets	Soft iron	Young's modulus of rotor and disk (E)	2×10^{11} N/m^2
Rotor	Structural steel	Poison ratio (ν)	0.3
Disk	Structural steel	Disk diameter (D_d)	0.5 m
Disk thickness (h)	0.05 m	MRF Newtonian viscosity (η_0)	0.11 Pa • s

Specifically, the current (I) and hydrodynamic force (F) response data of the COMSOL Multiphysics were imported to system identification toolbox in MATLAB, and parameters such as sampling time and identification model structure were set to identify mathematical model of this system. Based on the best fit of 95.18% from excitation current to hydrodynamic force, the transfer function could be expressed as follows

$$G_1(s) = \frac{1265s + 43.54}{s^2 + 1.615s + 0.05389} \tag{19}$$

On the other hand, the relationship between the hydrodynamic force (F) and rotor Y-axis displacement (Y) was derived from mathematical model of MRF bearing-rotor system. The specific transfer function was derived as

$$G_2(s) = \frac{36.73s + 1.815}{4.1s^4 + 3646s^3 + 818200s^2 + 5442s + 58.55} \tag{20}$$

PID controller of the active MRF bearing

Improved Gray Wolf (IGWO) optimization algorithm

The GWO is one of intelligent algorithms, which is motivated by hunting behavior and social ladder of gray wolves.[48] The overview of original GWO is provided below, followed by the improved method.

(1) Social hierarchy

The GWO algorithm defines four types of gray wolves: Alpha (α), Beta (β), Delta (δ), and Omega (ω). Alpha is the most suitable wolf, followed by Beta and Delta. Other wolves are not less important and conducted as Omega class.

(2) Encircling prey

The prey is surrounded by gray wolves during hunting, which can be expressed mathematically as

$$D = \left| C \times X_p(t) - X(t) \right| \tag{21}$$

$$X(t+1) = X_o(t) - A \times D \tag{22}$$

where t is present number of iterations, $\boldsymbol{A}$ and $\boldsymbol{C}$ are coefficient vectors. $\boldsymbol{X}_o$ is the position vector of the prey and $\boldsymbol{X}$ presents the position vector of wolf. The coefficient vectors are expressed by

$$A = 2a \times r_1 - a \tag{23}$$

$$C = 2r_2 \tag{24}$$

where r_1 and r_2 are random vectors in the range 1 to 0 and vector a is linearly reduced from 2 to 0 during iterations.

(3) Hunting

In the hunting stage, the best positions of Alpha wolves, Beta wolves and Delta wolves are used to find the best positions of wolves. The next location where wolves surround their prey is

$$D_\alpha = |C_1 \times X_\alpha(t) - X(t)| \quad D_\beta = |C_2 \times X_\beta(t) - X(t)| \quad D_\delta = |C_3 \times X_\delta(t) - X(t)| \tag{25}$$

$$X_1 = X_\alpha - A_1 \times D_\alpha \quad X_2 = X_\beta - A_2 \times D_\beta \quad X_3 = X_\delta - A_3 \times D_\delta \tag{26}$$

$$X_p(t+1) = \frac{X_1 + X_2 + X_3}{3} \tag{27}$$

where $\boldsymbol{X}_\alpha$, $\boldsymbol{X}_\beta$, and $\boldsymbol{X}_\delta$ are position vectors of the Alpha, Beta, and Delta wolves, respectively. $\boldsymbol{X}_1$, $\boldsymbol{X}_2$, and $\boldsymbol{X}_3$ present the distance and direction of the ω wolves towards the α, β, and δ wolves, respectively. $\boldsymbol{X}_p(t)$ is present position vector of ω wolves.

(4) Attacking prey

When the prey stops moving, the gray wolf finishes the hunting process by attacking. In order to simulate approaching prey, when the value of a decreases linearly from 2 to 0, its corresponding $\boldsymbol{A}$ also changes in the interval [-a, a].

$$a = 2 \times \left(1 - \frac{t}{N_{max}}\right) \tag{28}$$

where $N_{\max}$ is the maximum number of iterations.

(5) Searching the prey

When the value of $\boldsymbol{A}$ is within the range [-a, a], the next position of the gray wolf can be anywhere between its current position and the position of its prey. When $|\boldsymbol{A}| < 1$, wolves attacked their prey. When $|\boldsymbol{A}| > 1$, the gray wolf was separated from its prey, hoping to find more suitable prey. The positions of wolves are updated after each iteration and recalculate the positions of Alpha, Beta, Delta wolves to capture prey.

In this research, the convergence coefficient vectors a is evaluated by a nonlinear adjustment instead of linear change, which can increase local optimization ability in the middle and later stage of the algorithm. On the other hand, inspired by the particle swarm optimization algorithm, the individual can learn from the global optimal location and the historical optimal location at the same time. Based on this, a new improved location update rule is proposed. When inertia weight w is high, the global optimization ability of the algorithm is significantly reduced, but the local search is increased. When the inertia weight w is small, the global optimization ability is increased, while the local optimization is reduced. The specific position update methods are as follows

$$a = 2 - 2 \times ln\left(1 + (e-1) \times \frac{t}{N_{max}}\right) \tag{29}$$

$$X_p(t+1) = w \times \frac{X_1 + X_2 + X_3}{3} + m_1 \cdot r_1 \cdot \left(X_p - X\right) + m_2 \cdot r_2 \cdot \left(X_p - X\right) \tag{30}$$

$$w = \frac{N_{max}}{N_{max} \times \left(w_i - w_f\right) + w_f} \tag{31}$$

where m_1, m_2, w_i, and w_f are constant value, and they were set in this work: $m_1 = m_2 = 0.5$, $w_i = 2$, $w_f = 0$.

The IGWO can better balance the global and local optimizations and has better ability to jump out of local optimization. The flowchart of proposed IGWO algorithm is provided in Figure 6.

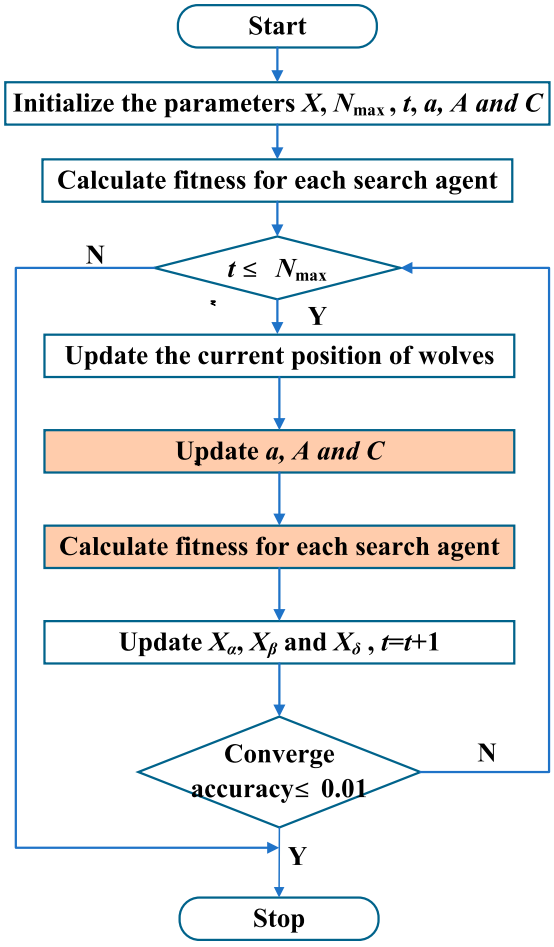

Figure 6. The flowchart of improved gray wolf optimization (IGWO) algorithm.

Feasibility verification of the IGWO algorithm

In order to verify the performance of the IGWO algorithm, it is necessary to calculate the optimal value of test functions. Consequently, this work selected four test functions of Sphere, Step, Griewank, and Rastrigin. The two algorithms have the same initial conditions, where the number of gray wolf population is 30, and the number of iterations is 500. The best optimal values are shown in Table 3 and their fitness values with the iterations are shown in Figure 7.

From Table 3 and Figure 7, IGWO algorithm has obvious advantages in convergence accuracy and the smaller optimal value compared with GWO. Therefore, it is proved that IGWO in this work effectively enhances the optimal value of original GWO with satisfactory convergence rate.

Simulation results

The validation of FEM model

In order to verify the present FEM model, experimental results presented in[24] are used for comparison. Consequently, this work uses the same modeling parameters: $D = 50$ mm, $L = 50$ mm, $C = 0.1$ mm, MRF-122-2ED, rotating speed (n) = 200 r/min. In this article, the bottom two coils are energized by current, and the magnetic field distribution of MR fluid journal bearing is shown in Figure 8. Clearly, the red arrow represents the direction of the magnetic field. Figure 8 shows that the magnetic field of the oil film below becomes stronger, and therefore can provide larger load capacity.

From the Figure 9, the numerical results obtained from the mathematical model in this work match experimental results in Ref [28] in the range of normal operational eccentricities, and hence it could be considered fully validated.

Table 3. The best optimal values of test functions.

Algorithm	Sphere	Step	Griewank	Rastrigin
GWO	1.4123e-24	0.013923	0.1222	4.5421
IGWO	3.1471e-244	2.6845e-05	0.0077865	0

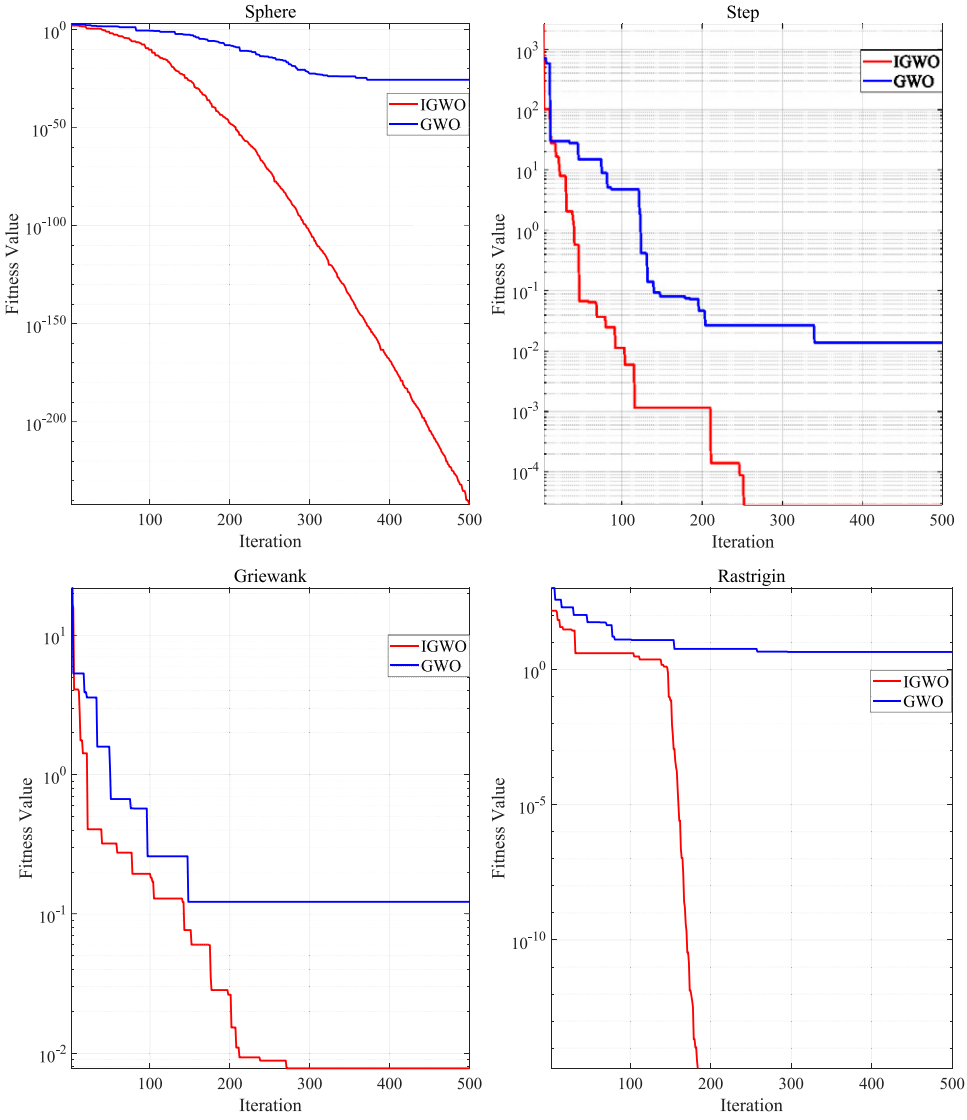

Figure 7. Comparison of fitness convergence curve.

The performance evaluation of MRF bearing-rotor system

The main purpose of designing this MRF bearing is to increase fluid-film bearing load capacity and reduce the displacement of the shaft, and therefore it can suppress rotor vibration and enhance the dynamic response of bearing-rotor system. The simulation of this system is operated in MATLAB/Simulink and set parameters: rotating speed (n) = 200 r/min, load (W) = 1000 N. The different magnetic induction intensities are 0, 25, and 50 mT in the bearing loading region, which are corresponding to different currents of 0, 1, and 2 A, respectively. As shown in Figure 10, when coil system is excited by current, the rotor center orbits are smaller than those without current. It is indicated that the active MRF bearing has larger minimum oil film thickness and it can avoid the direct contact between shaft and bearing and reduce friction. Under the

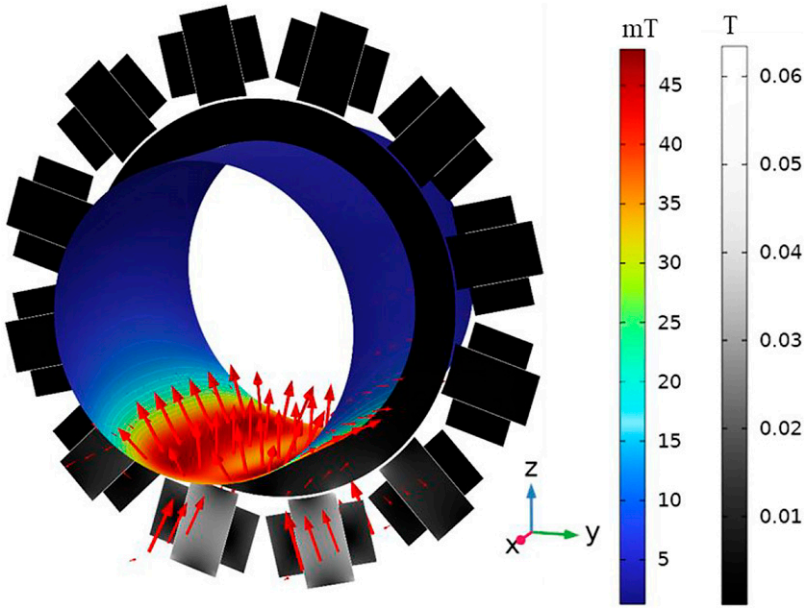

Figure 8. The magnetic field distribution of MR fluid journal bearing.

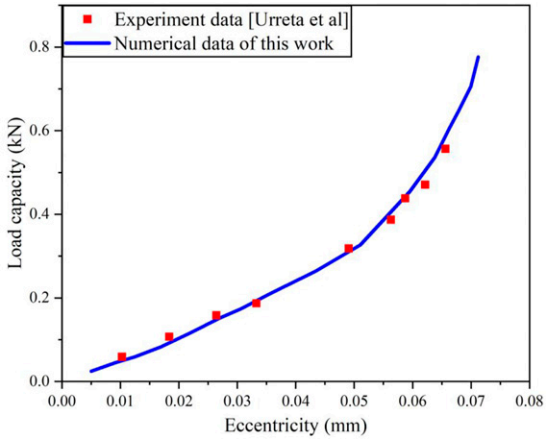

Figure 9. The validation of FEM model.

presence of magnetic field, the rotor stops the plane motion and stabilizes at a point in the final moment, and therefore the novel active bearing has ability to suppress rotor vibration, which could bring about oil whirl and whip phenomena. With the increasing of current magnitude, the orbit of shaft center is smaller, and hence it is possibility to further enhance rotating accuracy of shaft to adapt to more complex working conditions.

PID parameters optimized by different intelligent algorithms

In order to realize the smaller displacement of the shaft, it is fundamental to design an appropriate controller. So, the DC power is controlled by PID controller to produce magnetic field, which affects MRF viscosity. The parameters of PID are optimized by different intelligent algorithms. The principle of PID controller based on IGWO algorithm is shown in Figure 11. The $r(t)$ presents the ideal displacement of rotor and $Y(t)$ represents the actual rotor displacement. To evaluate various performance for the improved controller, the objective function ITAE is selected and expressed as

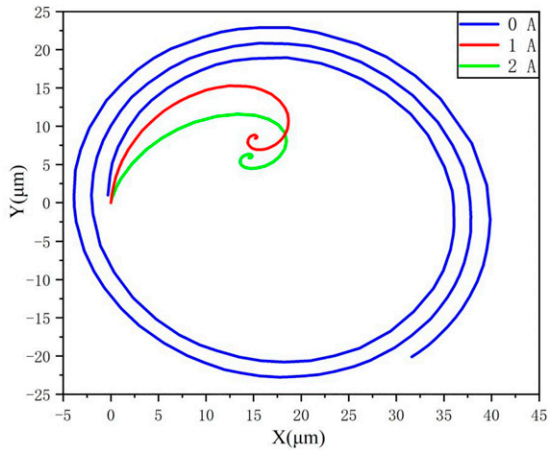

Figure 10. Comparison of the shaft center orbits under different currents.

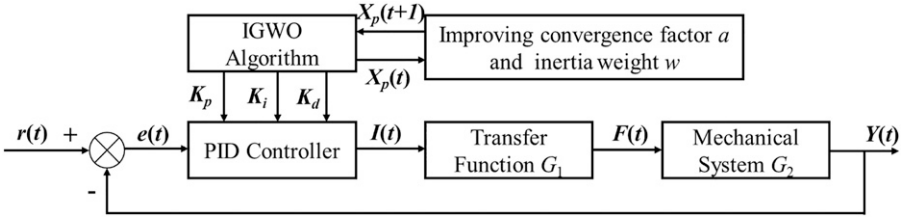

Figure 11. Principle of the PID controller based on IGWO algorithm.

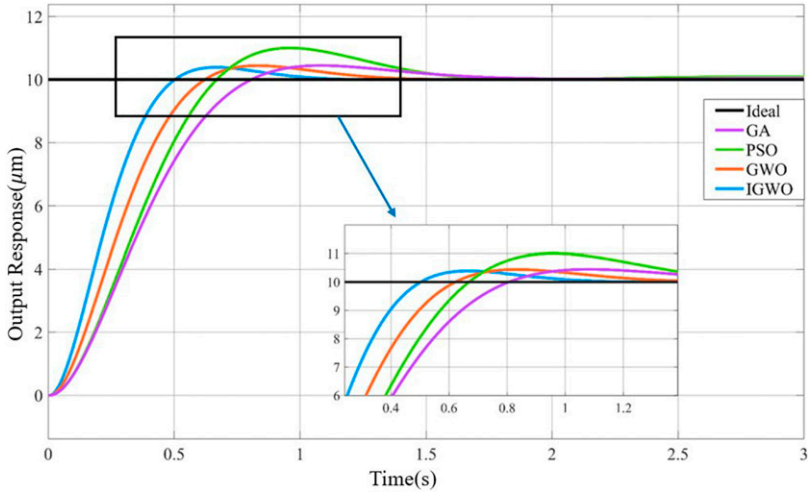

Figure 12. The output response of step signals based on different PID controller parameters.

Table 4. Performance indexes of the output response based on different PID controller parameters.

Controller type	K_p	K_i	K_d	t_r (0.1 to 0.9, s)	M_p (%)	t_s (±2%, s)
GA-PID	300	0.001	76.8	0.517	4.4	1.48
PSO-PID	299.2	4.59	61.48	0.446	10	1.5
GWO-PID	500	0.001	106.56	0.399	4.3	1.12
IGWO-PID	800	0.001	144.66	**0.320**	**3.8**	**0.87**

$$ITAE_{obj} = \int_0^{\infty} t|e(t)|dt \tag{32}$$

where $e(t)$ is error value and t is time.

GA-PID, PSO-PID, GWO-PID, and IGWO-PID controllers are used to simulate the response of step signal, which is set as 10 μm in this work and represents the ideal displacement of rotor. The simulation is operated in MATLAB/Simulink. The four intelligent optimization algorithms have the same parameter settings: $N_{\max} = 100$, $X = 30$. The responses of output are shown in Figure 12.

The detailed data about different PID controller parameters and their output responses are shown in Table 4. Simulation results show that IGWO-PID controller has best response speed, overshoot and steady-state error compared with GWO, PSO, and GA algorithms, and hence the IGWO algorithm can find the more appropriate PID controller parameters, that the validity of this algorithm is further proved.

Conclusions and future works

In this work, MRF as lubrication oil film adds an extra degree of freedom in the bearing than traditional fluid-film bearing. Therefore, a novel active MRF fluid-film bearing is designed and its intelligent lubrication mechanism is analyzed. The IGWO-PID controller is proposed to control this bearing more effectively so as to provide higher load capacity and suppress rotor vibration. Thus, contact and friction between shaft and bearing can be reduced, and their service life could be prolonged extremely. First, mathematical model of MRF bearing-rotor system is derived, and FEM model is utilized to obtain stiffness and damping coefficients to supplement mathematical model. Furthermore, an IGWO algorithm is developed to tune the PID parameters. Lastly, the simulation results show that with the increasing of current magnitude, the orbits of shaft center decrease. Under the action of magnetic field, the shaft of the novel active MRF fluid-film bearing can stabilize at a point in the final moment, and therefore this bearing has ability to suppress rotor vibration, which could bring about oil whirl and whip phenomena. In addition, IGWO-PID controller has better response characteristics than GWO, PSO, and GA algorithms, and hence the IGWO algorithm can find the more appropriate PID controller parameters, that the validity of this algorithm is further proved. The above conclusions are of reference significance for lubrication design, fault diagnosis and life predication of MRF fluid-film bearing.

Future work of this research will carry out physical tests to further verify the excellent load capacity of active MRF bearing under heavier load operating conditions. In addition, IGWO-PID controller may not be suitable since its robustness is insufficient under extremely heavy load conditions. Therefore, more advanced controllers will be used to further reduce displacement of shaft to adapt to various complex conditions.

Declaration of conflicting interests

The author(s) declared no potential conflicts of interest with respect to the research, authorship, and/or publication of this article.

Funding

The author(s) disclosed receipt of the following financial support for the research, authorship, and/or publication of this article: The support of National Natural Science Foundation of China (No. 51975568), Natural Science Foundation of Jiangsu Province (No. BK20191341), Jiangsu Funding Program for Excellent Postdoctoral Talent under Grant 2022ZB519, China Postdoctoral Science Foundation under Grant 2022M723387 and Priority Academic Program Development of Jiangsu Higher Education Institutions (PAPD) in carrying out this research are gratefully acknowledged. The research leading to these results has received funding from the Norwegian Financial Mechanism 2014-2021 under Project Contract No 2020/37/K/ST8/02748.

ORCID iD

Zhixiong Li https://orcid.org/0000-0002-7265-0008

Data Availability Statement

The data given this article can be requested from the corresponding author.

References

1. Hei D and Zheng MR. Investigation on the dynamic behaviors of a rod fastening rotor based on an analytical solution of the oil film force of the supporting bearing. *J Low Freq Noise Vib Active Control* 2021; 40: 707–739.
2. Gropper D, Wang L and Harvey TJ. Hydrodynamic lubrication of textured surfaces: a review of modeling techniques and key findings. *Tribol Int* 2016; 94: 509–529.
3. Aurelian F, Patrick M and Mohamed H. Wall slip effects in (elasto) hydrodynamic journal bearings. *Tribol Int* 2011; 44: 868–877.
4. Ibatan T, Uddin MS and Chowdhury MAK. Recent development on surface texturing in enhancing tribological performance of bearing sliders. *Surf Coat Technol* 2015; 272: 102–120.
5. Pattnayak MR, Pandey RK and Dutt JK. Performance behaviours of a self-acting gas journal bearing with a new bore design. *Tribol Int* 2020; 151: 106418.
6. Ramos DJ and Daniel GB. A new concept of active hydrodynamic bearing for application in rotating systems. *Tribol Int* 2021; 153: 106592.
7. Gad AM, Nemat-Alla MM, Khalil AA, et al. On the optimum groove geometry for herringbone grooved journal bearings. *J Tribol-T ASME* 2006; 128: 585–593.
8. Hashimoto H, Ochiai M, Hara H, et al. Optimization of groove geometry for thrust air bearing to maximize bearing stiffness. *J Tribol-T ASME* 2008; 130(3): 031101.
9. Cunha BZ and Daniel GB. Effects of bearing lubrication conditions on rotor dynamic behavior. *P I Mech Eng J-J Eng* 2022; 236: 563–580.
10. Brito FP, Miranda AS, Claro JCP, et al. Experimental comparison of the performance of a journal bearing with a single and a twin axial groove configuration. *Tribol Int* 2012; 54: 1–8.
11. Sharma SC and Ram N. Influence of micropolar lubricants on the performance of slot-entry hybrid journal bearing. *Tribol Int* 2011; 44: 1852–1863.
12. Agrawal A, Ciocanel C, Martinez T, et al. A bearing application using magnetorheological fluids. *J Intell Mater Syst Struct* 2002; 13: 667–673.
13. Wang NN, Liu XH and Zhang XH. Squeeze-strengthening effect of silicone oil-based magnetorheological fluid with nanometer Fe_3O_4 addition in high-torque magnetorheological brakes. *J Nanosci Nanotechnol* 2019; 19: 2633–2639.
14. Song WL, Li DH, Tao Y, et al. Simulation and experimentation of a magnetorheological brake with adjustable gap. *J Intell Mater Syst Struct* 2017; 28: 1614–1626.
15. Song Y, Guo SX, Yin XC, et al. Design and performance evaluation of a haptic interface based on MR fluids for endovascular tele-surgery. *Microsyst Technol* 2018; 24: 909–918.
16. Hua DZ, Liu XH, Sun SS, et al. Precise locomotion controller design for a novel magnetorheological fluid robot based on improved gray wolf optimization algorithm. *Smart Mater Struct* 2021; 30(2): 025038.
17. Nordin NHD, Muthalif AGA and Razali MKM. Control of transtibial prosthetic limb with magnetorheological fluid damper by using a fuzzy PID controller. *J Low Freq Noise Vib Active Control* 2018; 37: 1067–1078.
18. Munyaneza O and Sohn JW. Modeling and control of hybrid MR seat damper and whole body vibration evaluation for bus drivers. *J Low Freq Noise Vib Active Control* 2022; 41: 659–675.
19. Hegger C and Maas J. Smart sealing for magnetorheological fluid actuators. *J Intell Mater Syst Struct* 2019; 30: 689–700.
20. Zhou HL, Zhao W, Zhang HD, et al. Magnetorheological seal: a review. *Int J Appl Electromagn Mech* 2020; 62: 763–786.
21. Guo HY and Zhang L. Optimal placement of MR dampers for structural control using identification crossover genetic algorithm. *J Low Freq Noise Vib Active Control* 2004; 23: 167–178.
22. Hua DZ, Liu XH, Sun SS, et al. A magnetorheological fluid-filled soft crawling robot with magnetic actuation. *IEEE-ASME T Mech* 2020; 25: 2700–2710.
23. Hesselbach J and Abel-Keilhack C. Active hydrostatic bearing with magnetorheological fluid. *J Appl Phys* 2003; 93: 8441–8443.
24. Guldbakke JM and Hesselbach J. Development of bearings and a damper based on magnetically controllable fluids. *J Phys-Condens Mat* 2006; 18: S2959–S2972.
25. Gertzos KP, Nikolakopoulos PG and Papadopoulos CA. CFD analysis of journal bearing hydrodynamic lubrication by Bingham lubricant. *Tribol Int* 2008; 41: 1190–1204.

26. Bompos DA and Nikolakopoulos PG. CFD simulation of magnetorheological fluid journal bearings. *Simul Modell Pract Theory* 2011; 19: 1035–1060.
27. Sahu K and Sharma SC. A simulation study on the behavior of magnetorheological fluid on herringbone-grooved hybrid slot-entry bearing. *Tribol Trans* 2019; 62: 1099–1118.
28. Urreta H, Leicht Z, Sanchez A, et al. Hydrodynamic bearing lubricated with magnetic fluids. *J Intell Mater Syst Struct* 2010; 21: 1491–1499.
29. Bhat AK, Vaz N, Kumar Y, et al. Comparative study of journal bearing performance with ferrofluid and mr fluid as lubricant. In: International Conference on Emerging Trends in Mechanical Engineering (eTIME), India, 10–11 Aug 2018: Emerging Trends in Mechanical Engineering 2018.
30. Bompos DA, Nikolakopoulos PG and Asme. Experimental and analytical investigations of dynamic characteristics of magnetorheological and nano-magnetorheological fluid film journal bearing, In: ASME Turbo Expo: Turbine Technical Conference and Exposition Dusseldorf, Germany, 16–20 Jun 2014: Proceedings of the ASME Turbo Expo: Turbine Technical Conference and Exposition, 2014, vol 1b.
31. Bompos DA and Nikolakopoulos PG. Rotordynamic analysis of a shaft using magnetorheological and nanomagnetorheological fluid journal bearings. *Tribol Trans* 2016; 59: 108–118.
32. Wang XH, Li HG, Lu W, et al. Stiffness and damping properties of (semi) floating ring bearing using magnetorheological fluids as lubricant. *J Tribol-T ASME* 2017; 139(5): 051701.
33. Wang XH, Li HG and Meng G. Rotordynamic coefficients of a controllable magnetorheological fluid lubricated floating ring bearing. *Tribol Int* 2017; 114: 1–14.
34. Quinci F, Litwin W, Wodtke M, et al. A comparative performance assessment of a hydrodynamic journal bearing lubricated with oil and magnetorheological fluid. *Tribol Int* 2021; 162: 107143.
35. Urreta H, Aguirre G, Kuzhir P, et al. Actively lubricated hybrid journal bearings based on magnetic fluids for high-precision spindles of machine tools. *J Intell Mater Syst Struct* 2019; 30: 2257–2271.
36. Solís-Pérez J, Gómez-Aguilar JF, Hernández J, et al. Global optimization algorithms applied to solve a multi-variable inverse artificial neural network to improve the performance of an absorption heat transformer with energy recycling. *Appl Soft Comput* 2019; 85: 105801.
37. Chávez-Vázquez S, Lavín-Delgado JE, Gómez-Aguilar JF, et al. Trajectory tracking of Stanford robot manipulator by fractional-order sliding mode control. *Appl Math Modell* 2023; 120: 436–462.
38. Gulbahce E and Celik M. Active vibration control of a smart beam by a tuner-based PID controller. *J Low Freq Noise Vib Active Control* 2018; 37: 1125–1133.
39. Sen MA, Tinkir M and Kalyoncu M. Optimisation of a PID controller for a two-floor structure under earthquake excitation based on the bees algorithm. *J Low Freq Noise Vib Active Control* 2018; 37: 107–127.
40. Nicoletti R and Santos IF. Linear and non-linear control techniques applied to actively lubricated journal bearings. *J Sound Vib* 2003; 260: 927–947.
41. Qiu J, Tani J and Kwon T. Control of self-excited vibration of a rotor system with active gas bearings. *J Vib Acoust* 2003; 125: 328–334.
42. Laldingliana J and Biswas PK. Artificial intelligence based fractional order PID control strategy for active magnetic bearing. *J Electr Eng Technol* 2022; 17: 3389–3398.
43. Bordoloi DJ and Tiwari R. Optimization of controller parameters of active magnetic bearings in rotor-bearing systems. *Adv Vib Eng* 2013; 12: 319–327.
44. Gupta S, Biswas PK, Babu TS, et al. Hunting based optimization techniques used in controlling an active magnetic bearing system. *IEEE Access* 2022; 10: 62702–62721.
45. Wang NN, Liu XH, Sun SS, et al. Microscopic characteristics of magnetorheological fluids subjected to magnetic fields. *J Magn Magn Mater* 2020; 501: 1–11.
46. Shen YR, Hua DZ, Liu XH, et al. Visualizing rheological mechanism of magnetorheological fluids. *Smart Mater Struct* 2022; 31(2): 025027.
47. Lord Corporation. Lord technical data: MRF-132DG magneto-rheological fluid. http://www.lord.com
48. Mirjalili S, Mirjalili SM and Lewis A. Grey wolf optimizer. *Adv Eng Software* 2014; 69: 46–61.